JOURNAL OF AIRCRAFT
Vol. 47, No. 4, July–August 2010

Full-Configuration Drag Estimation

Ohad Gur,* William H. Mason,† and Joseph A. Schetz‡
Virginia Polytechnic Institute and State University, Blacksburg, Virginia 24061-0203

DOI: 10.2514/1.47557

Accurate drag estimation is critical in making computational design studies. Drag may be estimated thousands of times during a multidisciplinary design optimization, and computational fluid dynamics is not yet possible in these studies. The current model has been developed as part of an air-vehicle conceptual-design multidisciplinary design optimization framework. Its use for subsonic and transonic aircraft configurations is presented and validated. We present our parametric geometry definition, followed by the drag model description. The drag model includes induced, friction, wave, and interference drag. The model is compared with subsonic and transonic isolated wings, and a wing/body configuration used previously in drag prediction workshops. The agreement between the predictions of the drag model and test data is good, but lessens at high lift coefficients and high transonic Mach numbers. In some cases the accuracy of this drag estimation method exceeds much more elaborate analyses.

Nomenclature

AR	=	aspect ratio
a, b	=	superellipse half-axes
$C_{D,F}$	=	friction-drag coefficient
C_{Di}	=	three-dimensional induced-drag coefficient
$C_{D\,\mathrm{int}}$	=	three-dimensional interference-drag coefficient
C_{Dw}	=	three-dimensional wave-drag coefficient
C_{di}	=	two-dimensional induced-drag coefficient
C_L	=	three-dimensional lift coefficient
C_l	=	two-dimensional lift coefficient
$C_{l\alpha}$	=	two-dimensional lift-coefficient slope
C_n	=	two-dimensional normal-force-coefficient slope
c	=	local chord length
c_{avg}	=	average chord length
$\mathrm{d}l$	=	bound vortex length
FF	=	fuel flow
M	=	Mach number
M_{cr}	=	critical Mach number
M_{DD}	=	drag divergence Mach number
m, n	=	superellipse powers
Re_c	=	chord Reynolds number
$Re_{c_{\mathrm{avg}}}$	=	average chord Reynolds number
Re_l	=	Reynolds number based on length l
S_{ref}	=	reference area
S_{wet}	=	wetted area
TF	=	technology factor
t/c	=	streamwise thickness-to-chord ratio
u_∞	=	freestream airspeed
v_i	=	induced velocity
$\mathbf{W}$	=	aerodynamic influence matrix
$(x/c)_m$	=	chordwise position of maximum thickness
y, z	=	coordinates
y_c, z_c	=	superellipse origin coordinates
α	=	angle of attack
α_g	=	geometric angle of attack
α_i	=	induced angle of attack
Γ	=	circulation
θ	=	pitch angle
κ_A	=	Korn airfoil technology factor
Λ_{LE}	=	leading-edge sweep angle
Λ_m	=	maximum thickness line sweep angle
$\Lambda_{0.25}$	=	quarter-chord sweep angle
$\Lambda_{0.5}$	=	half-chord sweep angle
λ	=	taper ratio
ρ	=	density
ϕ	=	wing/body intersection angle

Subscripts

body	=	body coefficient
H	=	Hoerner model
i	=	induced
J	=	Jobe model
k, p	=	indices
L	=	lower
N	=	Nicolai model
R	=	Raymer model
S	=	Shevell model
T	=	Torenbeek model
U	=	upper
wing	=	wing coefficient

I. Introduction

AERODYNAMICISTS have been looking for practical and efficient ways to estimate drag since the first days of aeronautics. These efforts resulted in empirical methods such as Hoerner's drag estimation methods [1] and other methods such as Prandtl's landmark lifting-line model [2,3]. These methods were developed for aerodynamic analysis before the computer era.

Today, computational fluid dynamics (CFD) is widely used in aerodynamics. By discretizing the governing flowfield equations (whether potential, Euler, or Reynolds-averaged Navier–Stokes, etc.) the entire flowfield is found. Thus, CFD is invaluable in providing an understanding of the various flowfield phenomena. However, it is time-consuming to use in the early stages of design. In particular, the difficulty of embedding automatic, accurate, and reliable grid methodology within a multidisciplinary design optimization (MDO) methodology remains. This is especially true for complete three-dimensional configuration drag prediction, in which thousands of calculations are needed when embedding CFD in a computational design approach such as MDO. Numerous efforts are being made to predict drag using CFD accurately [4–7], but it is still difficult and considered a challenge. We have previously discussed these issues relevant to MDO [8], as well as presented a methodology that can be used once a configuration design has progressed to the

Presented as Paper 2009-4109 at the 27th AIAA Applied Aerodynamics Conference, San Antonio, TX, 22–25 June 2009; received 7 October 2009; revision received 26 January 2010; accepted for publication 22 February 2010.

*Research Associate, Aerospace and Ocean Engineering Department. Member AIAA.

†Professor, Aerospace and Ocean Engineering Department. Associate Fellow AIAA.

‡Holder of the Durham Chair, Aerospace and Ocean Engineering Department. Life Fellow AIAA.

point that CFD is needed [9]. Finally, the analytic methodology developed in the past has provided the relationships and functional forms of key drag parameters that are not available in CFD but are critical to understanding how to design for low drag.

Paterson et al. [10] presented a description of semi-empirical drag prediction techniques used at Lockheed. Although this survey was made more than 30 years ago, it demonstrated good agreement with test data and can still be used for current drag estimation. Filippone [11] recently presented a comprehensive survey of drag prediction for transport aircraft based on semi-empirical models. He then demonstrated his method by calculating the performance of a Boeing 747 with good accuracy.

Air-vehicle conceptual design is based mainly on performance goals and other design constraints (structural, controls, cost, etc.) [12,13]. Within this context, one of the main challenges in conceptual design is finding the vehicle performance as a function of the vehicle outer-mold-line geometry. The vehicle's performance characteristics are directly related to its drag polar; thus, finding the drag polar is a major effort within the design process. Each design perturbation will influence the vehicle geometry, thus requiring a new estimation of the drag polar. Using CFD directly within a conceptual-design process is still impractical.

The current paper describes a drag estimation method suitable for use in the MDO design of transonic airplanes. The purpose of the model is to give fast and accurate drag estimation within the MDO design process. In this context, the parametric geometry of the configuration is important, so it is described first.

Next, the drag estimation method based on a variety of simple theoretical and semi-empirical models and targeted CFD results is presented. The final model is then validated using three different wind-tunnel tests: an unswept isolated subsonic wing [14], an isolated swept transonic wing [15], and a simple fuselage/wing/body configuration [16] used previously in the drag prediction workshop series [5–7]. Although it is simple, the present model gives reliable drag estimations for the lower-Mach-number transonic regime and moderate lift coefficient; thus, it is suitable for use in MDO conceptual design. In addition, current research efforts use a combination of classical low-fidelity and advanced high-fidelity methods in a multilevel approach [17]. The presented method is a good candidate for the low-fidelity part in these multilevel approaches.

II. Parametric Geometry

An essential part of aerodynamic analysis is a precise geometry definition. The boundary conditions for aerodynamic analysis are based on these definitions, so it is an important part of the analysis process. Conducting numerous different configuration analyses requires the use of parametric geometry, using a small number of parameters to accurately represent a variety of configuration shapes. One of the current uses of parametric geometry is within optimization design processes that use the parameters as design variables. This puts an emphasis on using a small number of parameters.

Examples of such processes can be found in airfoil designs using shape-function parametric geometry [18–20]. In these examples, the airfoil contour is defined by superposition of one-dimensional shape functions. Each shape function is weighted differently, and thus the weight coefficients are used as design variables. Shape-function methods are also used for more complicated geometry, including full configurations: for example, Vachris and Yaeger's [21] quick-geometry method and Kulfan's [22] CST (class-function/shape-function transformation). The main advantage of using shape functions is the accurate definition of complex geometry using a small number of design variables with an analytic formulation. This makes shape functions natural candidates for parametric geometry in CFD analysis.

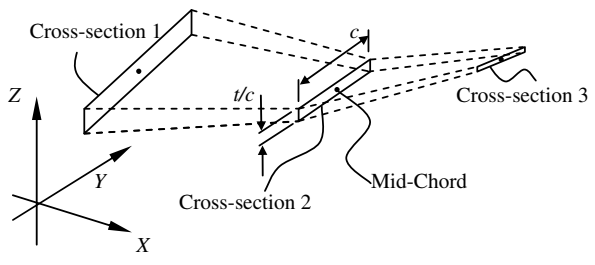

Fig. 1 Parametric geometry representation of a wing.

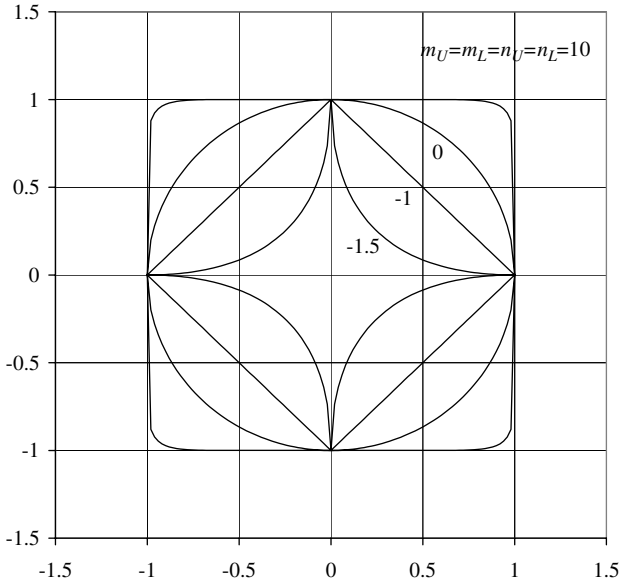

Fig. 2 Superellipse sections used for fuselage-type shapes; a_U, a_L, b_U, and $b_L = 1.0$.

For the present drag estimation method, which is not based on CFD analysis, simpler methods should be considered, such as Rodriguez and Sturdza's [23] RAGE (rapid-geometry engine). In this method, two main entities are defined: winglike surfaces (wing, horizontal/vertical tail, etc.) or bodies (fuselage, nacelle, external fuel tank, etc.). RAGE defines the wing surfaces by lofting between airfoils prescribed at a small number of wing stations. In a similar way, bodies are defined by lofting between fuselagelike cross sections. Barger [24] provided an excellent mathematical approach for such a lofting procedure. Note that RAGE is also being used for CFD analysis, although it is somewhat simpler than CST.

Filippone [11] used a simpler method that makes use of the wing planform and equivalent bodies of revolution for fuselage representation. This geometry is somewhat less versatile than CST or RAGE and essentially applies to transport configurations. Although it is a more basic representation, Filippone's method exhibits good results for drag estimation and performance calculation.

A different approach[§] is based on parameterization of the wing/body using geometrical properties such as span, aspect ratio, area, length, etc. [25]. This kind of parametric geometry only suits conventional configurations and presents some limitations for other more elaborate designs.

The current research uses RAGE-like parametric geometry. The wings are constructed by linearly joining two or more cross sections (Fig. 1). The cross sections are defined by their midchord spatial position, rotation angles of the section around its midchord, chord length c and thickness ratio t/c. Although this parametric geometry is not capable of precisely describing continually curving planforms (e.g., an elliptic wing), it is capable of representing such surfaces with sufficient accuracy using a number of trapezoid surfaces. On the other hand, this representation enables the usage of straight trailing edges, thus eliminating trailing-edge warping due to a linear twist-angle distribution.

A similar approach is used for the parametric geometry of bodies. Multiple cross sections are connected linearly, so that general body configurations can be defined. The body sections are defined by the upper and lower parts of a superellipse (Lamé curve). For a two-dimensional plane, Y-Z, the coordinates y and z of the superellipse are defined using the following relation:

[§]Data available online at http://www.avidaerospace.com/.

$$z = \begin{cases} z_c + b_U\left[1 - \left(\frac{|y-y_c|}{a_U}\right)^{2+m_U}\right]^{\frac{1}{2+n_U}} & y_c - a_U < y < y_c + a_U \text{ (upper part)} \\ z_c - b_L\left[1 - \left(\frac{|y-y_c|}{a_L}\right)^{2+m_L}\right]^{\frac{1}{2+n_L}} & y_c - a_L < y < y_c + a_L \text{ (lower part)} \end{cases} \quad (1)$$

where (y_c, z_c) are the origin coordinates; a_U and a_L are the horizontal half-axis lengths of the upper and lower parts, respectively; b_U and b_L are the vertical half-axis lengths of the upper and lower parts, respectively; and $m_U, m_L.n_U$, and n_L are the superellipse powers that control the cross sectional shape.

Figure 2 presents four different superellipses having a_U, a_L, b_U, and $b_L = 1.0$ and using various powers $m_U = m_L = n_U = n_L$. For $m_U = m_L = n_U = n_L = 0$ the superellipse is a circle, $m_U = m_L = n_U = n_L = -1.0$ makes it a diamond shape, $m_U = m_L = n_U = n_L < -1.0$ demonstrates a chine shape, and $m_U = m_L = n_U = n_L \to \infty$ leads to a square-shaped section. These examples exhibit the versatility of using superellipse curves.

This parametric geometry enables a conventional fuselage/wing representation as well as more complicated geometries such as a joined wing, as presented in Fig. 3. Note that this figure was produced using the NASA-developed Vehicle Sketch Pad (VSP), which is an extension of the rapid aircraft modeler [25]. The current parametric geometry can be imported into VSP, which enables a quick visualization of various configurations [26].

III. Drag Model

It is common to divide a configuration's total drag into two components: induced and parasite. Several nomenclatures can be found for the parasite-drag breakdown [10,11,27], whereas the current research uses three components: friction/form, interference, and wave drag. Figure 4 shows the drag breakdown into its various components.

Each of the parasite-drag components include the influence of lift; thus, the parasite drag cannot be defined as the zero-lift drag. Still, the influence of lift on the total parasite drag is generally small.

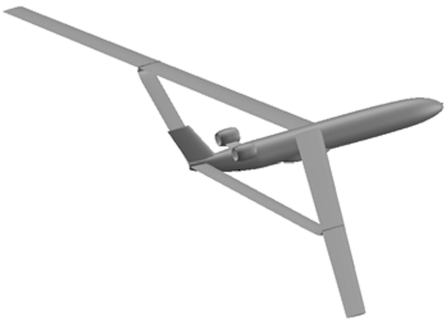

Fig. 3 Geometry visualization of a joined-wing configuration using VSP.

The following sections describe the different components within the drag breakdown and illustrate the models being used to estimates these components.

A. Induced Drag

Induced drag often contributes about half of the entire vehicle drag, and thus accurate induced-drag modeling is essential. Several induced-drag models exist, such as the Trefftz plane [28], Prandtl's lifting-line theory [2,3], and the vortex lattice method [29]. The current research uses a Weissinger nonlinear lifting-line model [30–32]. This method takes advantage of two-dimensional lift data, and thus the viscosity and compressibility effects can be included, although the model was originally developed for linear aerodynamics and incompressible flow. The airfoil two-dimensional lift data only contributed at high-lift conditions, well away from most conditions of interest. Thus, a linear 2-D lift model can be used at low-lift conditions, and in some cases, the theoretical lift-slope value 2π can be used. Note that the current model does not make use of the two-dimensional airfoil drag data. These data are sometimes of low reliability, as demonstrated in [33] for the NACA-0012 airfoil. The airfoil drag is calculated using the friction/form drag model. A detailed description of the method that is used in the current model is given in [34].

B. Friction/Form Drag

According to the drag breakdown shown in Fig. 4, the friction/form drag can be divided into three components: skin friction, pressure, and lift-related profile drag. The current model neglects the third component, which is small, and the remaining two components are addressed simultaneously. The friction/form drag coefficient $C_{D,F}$ is calculated using the following relation for each component:

$$C_{D,F} = C_F \mathrm{FF} \frac{S_{\mathrm{wet}}}{S_{\mathrm{ref}}} \quad (2)$$

where C_F is a flat-plate skin-friction coefficient, FF is the form factor of the component, and S_{wet} and S_{ref} are the wetted and reference areas, respectively.

The full configuration is divided into components, and Eq. (2) is used separately for each component. Finally, the total friction/form drag is found by summing the contributions of these components. The current model divides the wings into strips, and each of these strips is treated as a separate component. The wetted area of each strip is found according to its chord and strip width. Bodies are treated differently: each body (fuselage, nacelle, fuel tank, etc.) is a single component with its own wetted area.

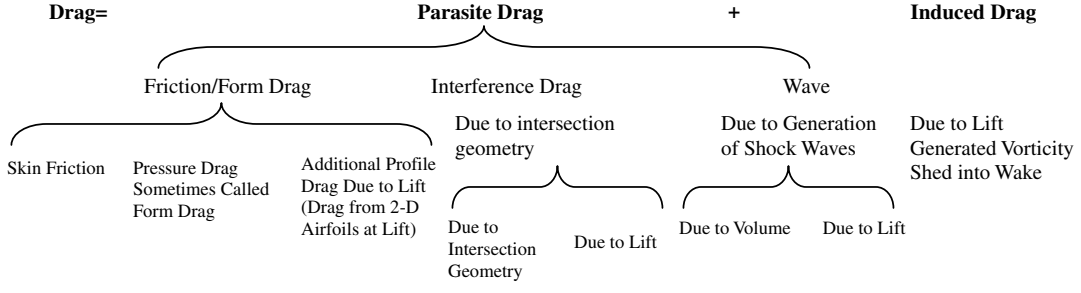

Fig. 4 Typical drag breakdown terminology.

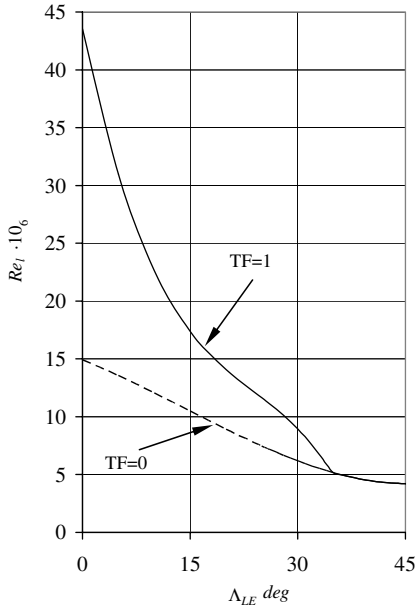

Fig. 5 Transition Reynolds number and technology factor definition [44].

For each component, the reference area and wetted areas are well-defined, but the flat-plate skin-friction coefficient and the form factor are estimated based on semi-empirical models. Various skin-friction and form-factor models exist in the literature [1,35,36]. Comparison of these models reveals small differences [10], and thus we chose the most well-known and validated models for the current method.

For laminar flow, the Eckert reference temperature method [37] is used, and for turbulent flow, the Van Driest II method [38,39] (based on the von Kármán–Schoenherr model) is used. The total skin-friction coefficient is based on a composition of the laminar/turbulent flow. Similar to the skin-friction models, several composition formulas are available [40,41], and Schlichting's composition formula [42] is used for the current research. The complete rigorous model for the flat-plate skin-friction coefficient can be found in [43].¶

For cases with natural transition, a simple method is used to determine the chordwise location of the boundary-layer transition. Figure 5 presents two curves of transition Reynolds number based on the chordwise Reynolds number, Re_l (taken from [44]). The dashed curve designated as TF = 0 (technology factor of 0) is for natural laminar flow on standard wings [45]. The solid curve, designated as TF = 1, refers to natural-laminar-flow airfoils [46]. For the current validation cases, we used TF = 0.

Form factor FF represents the drag correction due to thickness and pressure drag, which is sometimes referred to as profile drag, which contains skin friction and pressure drag. The current model makes use of two basic form factors: wing (FF_{wing}) and body of revolution (FF_{body}). Although other form factors exist [47], these two cover most of the drag estimation requirements for airplane configurations. The authors find it helpful to present a short review of several form-factor models, for both wings and bodies of revolution. The literature contains many different models from which the following will be considered here: Hoerner [1], Torenbeek [47], Jobe [48], Shevell [49], Nicolai [50], and Raymer [51].

Hoerner's [1] wing form-factor model is a function of the thickness ratio t/c:

$$\mathrm{FF}_{\mathrm{wing},H} = 1 + 2\frac{t}{c} + 60\left(\frac{t}{c}\right)^4 \tag{3}$$

The linear term is considered as the supervelocity correction (due to the airfoil thickness), and the quartic term represents the adverse pressure drag.

¶Data available online at http://www.aoe.vt.edu/~mason/Mason_f/FRICTman.pdf [retrieved 1 April 2009].

A similar wing form-factor model with different constants is suggested by Torenbeek [47]:

$$\mathrm{FF}_{\mathrm{wing},T,J} = 1 + 2.7\frac{t}{c} + 100\left(\frac{t}{c}\right)^4 \tag{4}$$

Jobe [48] expands this model to include the chordwise position of the maximal thickness $(x/c)_m$. For a typical airfoil using $(x/c)_m = 0.3$ (e.g., four-digit NACA series), Jobe's form factor is identical to Torenbeek's [47].

Some other more elaborate models are given by Shevell [49], Nicolai [50], and Raymer [51]. Shevell's model depends on the freestream Mach number M and the quarter-chord sweep angle $\Lambda_{c/4}$:

$$\mathrm{FF}_{\mathrm{wing},S} = 1 + \frac{(2-M^2)\cos\Lambda_{0.25}}{\sqrt{1-M^2\cos^2\Lambda_{0.25}}}\frac{t}{c} + 100\left(\frac{t}{c}\right)^4 \tag{5}$$

Nicolai [50] and Raymer [51] suggest a model that uses the airfoil maximal thickness $(x/c)_m$:

$$\mathrm{FF}_{\mathrm{wing},N,R} = \left[1 + \frac{0.6}{(x/c)_m}\frac{t}{c} + 100\left(\frac{t}{c}\right)^4\right] \cdot [1.34M^{0.18}(\cos\Lambda_m)^{0.28}] \tag{6}$$

where Λ_m is the maximum thickness line sweep, which is often close to the quarter-chord sweep line.

For unswept wings, $(x/c)_m = 0.3$, and low speed ($M = 0$ for Shevell and $M = 0.2$ for Nicolai/Raymer), both Eqs. (5) and (6) collapse to

$$\mathrm{FF}_{\mathrm{wing},N,R} = 1 + 2\frac{t}{c} + 100\left(\frac{t}{c}\right)^4 \tag{7}$$

Figure 6 presents a comparison between the above models [Eqs. (3), (4), and (7)]. The range of the form-factor values for a typical $t/c = 0.12$ airfoil is $1.25 < \mathrm{FF}_{\mathrm{wing}} < 1.35$, which suggests less than a 10% difference.

A similar comparison is presented for body-of-revolution form factors, in which the same references were used. All only depend on the body fineness ratio, which is defined as the ratio between the body length and its maximum diameter: l/d. Although length l and maximum diameter d are well-defined for fuselages, the proper fineness ratio is more ambiguous for nacelles or boat-tailed bodies [47].

All of the following models contain the same two terms that appear in the wing form factor: one for supervelocity and one for adverse pressure. The Hoerner [1] model is

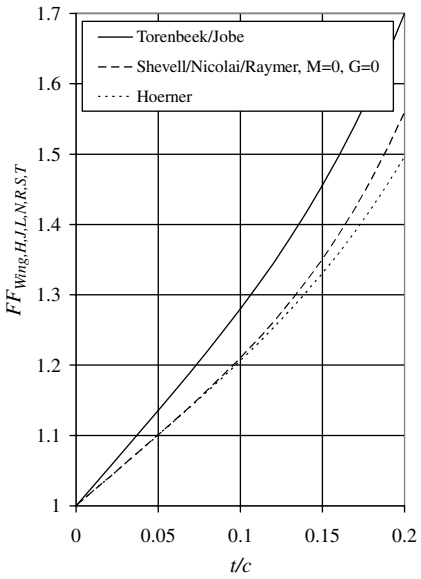

Fig. 6 Comparison of wing form factors for different thickness ratios.

$$\mathrm{FF}_{\mathrm{body},H} = 1 + \frac{1.5}{(l/d)^{1.5}} + \frac{7}{(l/d)^3} \tag{8}$$

The Torenbeek [47] model is

$$\mathrm{FF}_{\mathrm{body},T} = 1 + \frac{2.2}{(l/d)^{1.5}} + \frac{3.8}{(l/d)^3} \tag{9}$$

Jobe [48], Nicolai [50], and Raymer [51] share the same model:

$$\mathrm{FF}_{\mathrm{body},J,N,R} = 1 + 0.0025(l/d) + \frac{60}{(l/d)^3} \tag{10}$$

and the Shevell [49] model is

$$\mathrm{FF}_{\mathrm{body},S} = 1 + \frac{2.8}{(l/d)^{1.5}} + \frac{3.8}{(l/d)^3} \tag{11}$$

The results from these models are illustrated in Fig. 7. The difference between the various models for high-fineness-ratio bodies of revolution ($l/d = 10$) are small ($1.05 < \mathrm{FF}_{\mathrm{body}} < 1.09$). For lower-fineness-ratio bodies ($l/d = 4$) the difference between the models is more significant ($1.3 < \mathrm{FF}_{\mathrm{body}} < 1.95$).

C. Interference Drag

Interference drag arises from the intersection of a lifting surface and body or the intersection between two lifting surfaces. Various studies have been conducted analyzing such mutual interference (for a thorough literature review, see [52]). Although various types of intersections exist (wing/fuselage, wing/wing, strut/wing, etc.), only wing/fuselage interference drag is considered here. The model uses a combination of two interference-drag models: a CFD-based model from Tétrault et al. [53] and Hoerner's empirical model [1].

The CFD-based model relates to thin wings ($t/c < 0.075$) and is based on RANS CFD analysis, leading to the following response surface:

$$\begin{aligned} C_{D\,\mathrm{int}}\frac{S_{\mathrm{ref}}}{c^2} &= 0.1112 - 0.2572\sin\phi + 3.440t/c - 0.02097\log_{10}Re_c \\ &+ 0.09009\sin^2\phi - 2.549t/c\sin\phi + 0.03010\log_{10}Re_c\sin\phi \\ &- 0.1462t/c\log_{10}Re_c \end{aligned} \tag{12}$$

where Re_c is the Reynolds number based on the wing chord c at the intersection and ϕ, which is the inclination angle defined as the angle between the wing to a normal to the surface. This model is applicable only for small thickness ratios ($t/c < 0.075$), so it can used only for a wing/wing or wing/body intersection of very thin wings.

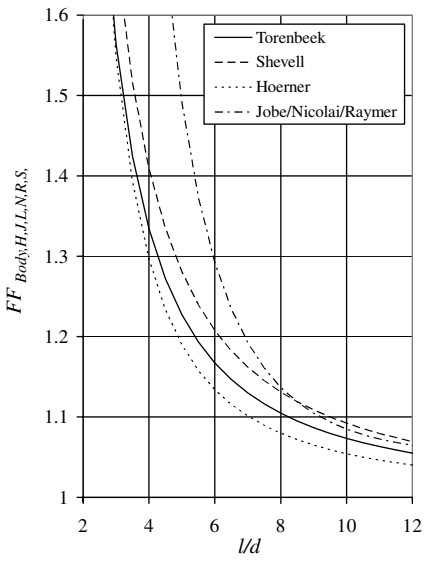

Fig. 7 Comparison between different body-of-revolution form factors.

The Hoerner model is based on subsonic, incompressible, viscous test data for high-thickness wings. For example, the inclination angle ϕ influence is based on a wind-tunnel test using a $t/c = 0.43$ wing. Additional influence parameters are the wing two-dimensional coefficient C_l, thickness ratio t/c, and quarter-chord sweep angle $\Lambda_{0.25}$. Because of the high thickness ratios, this model is suitable only for thick-wing/wing or wing/body interactions.

To create a model for reasonable wing thicknesses, the two models are used together. A linear interpolation is made according to the wing thickness ratio between the CFD-based model for $t/c = 0.075$ and the Hoerner model for $t/c = 0.4$. Although the two models are very different, this interpolation enables the calculation of intermediate thickness ratios, which characterize most current wing/fuselage and wing/wing configurations.

D. Wave Drag

Drag increase due to compressibility effects appears at airspeeds higher than the critical Mach number M_{cr}, due to shock waves. The current research deals with subsonic configurations; thus, the drag rise at transonic ($M < 1$) conditions is of interest. Figure 8 presents a typical wave-drag coefficient C_{Dw} increase for the DC-9-30 [54] as a function of the freestream Mach number M. Above the critical Mach number, the drag increase has a moderate slope (drag creep), and at higher Mach numbers (the drag divergence Mach number M_{DD}) the drag slope $\mathrm{d}C_{Dw}/\mathrm{d}M$ experiences a sudden increase. Figure 8 shows two definitions for the drag divergence Mach number M_{DD}. The first is defined as the Mach number that causes a 20-drag-count increase ($C_{Dw} = 0.002$). The second is defined using the drag-increase slope:

$$\frac{\mathrm{d}C_{Dw}}{\mathrm{d}M}\Big|_{M=M_{\mathrm{DD}}} = 0.1 \tag{13}$$

According to Fig. 8, the difference between the results of these two definitions is small.

The same criteria can be taken for a two-dimensional airfoil drag-coefficient slope, $\mathrm{d}C_{dw}/\mathrm{d}M$:

$$\frac{\mathrm{d}C_{dw}}{\mathrm{d}M}\Big|_{M=M_{\mathrm{DD}}} = 0.1 \tag{14}$$

According to [55,56], the drag rise can be modeled as the following function of the Mach number (Lock's fourth power law):

$$C_{dw} = \begin{cases} 0 & M \le M_{\mathrm{cr}} \\ 20(M - M_{\mathrm{cr}})^4 & M > M_{\mathrm{cr}} \end{cases} \tag{15}$$

The contribution of the wave drag on a wing strip relative to the total three-dimensional wave drag is calculated using the area ratio S_c/S_{ref}:

$$C_{Dw} = C_{dw}\frac{S_c}{S_{\mathrm{ref}}} \tag{16}$$

where S_c is the area of the wing strip represented by the two-dimensional cross section.

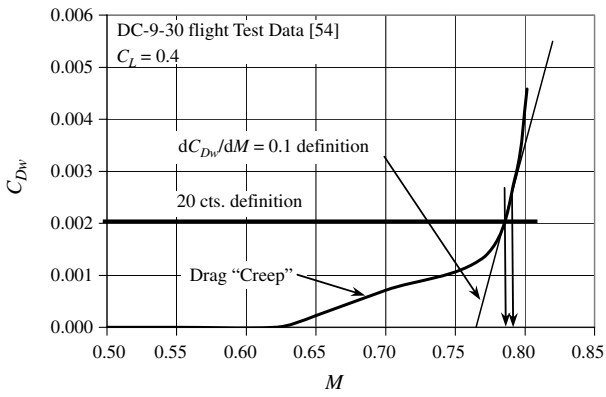

Fig. 8 Wave drag increase at transonic airspeeds.

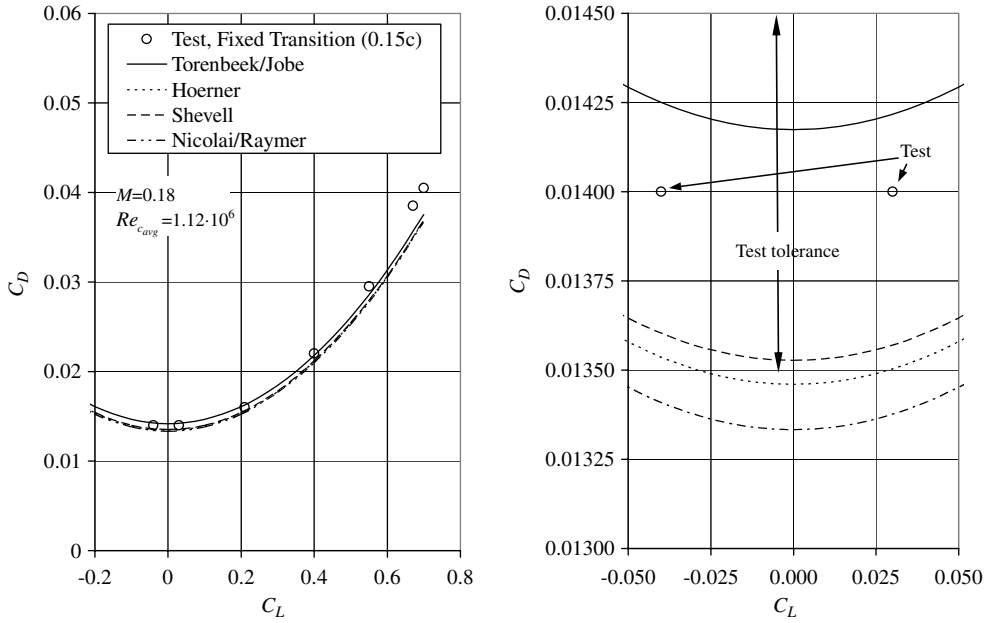

Fig. 9 Comparison between Smith's [14] drag data and the current model predictions using different form factors. Expanded scale region near $C_L = 0$ shown on the right.

Substituting Eq. (15) into Eq. (13) gives the following estimation for the critical Mach number M_{cr}:

$$M_{\text{cr}} = M_{\text{DD}} - \sqrt[3]{\frac{0.1}{80}} \tag{17}$$

This implies that the critical Mach number M_{cr} is lower than the drag divergence Mach number by a constant 0.108. The drag divergence Mach number M_{DD} for a specific wing cross section is found using the Korn equation extended with simple sweep theory [57]:

$$M_{\text{DD}} \cos \Lambda_{0.5} + \frac{C_l}{10\cos^2 \Lambda_{0.5}} + \frac{t/c}{\cos \Lambda_{0.5}} = \kappa_A \tag{18}$$

where $\Lambda_{0.5}$ is the midchord sweep angle and κ_A is the Korn factor. For supercritical airfoils, $\kappa_A = 0.95$, and for conventional airfoils, $\kappa_A = 0.87$. The validation of Eq. (18) is given in [57] for various thickness ratios, lift coefficients, and airfoil types.

The present wave-drag calculation procedure starts by dividing the wing into strips, as in the friction-drag calculation. Each strip is represented by its two-dimensional thickness ratio t/c, lift coefficient C_l, and half-chord sweep $\Lambda_{0.5}$. Then the drag divergence Mach number is calculated using Eq. (18). Note that this calculation includes the local lift coefficient, and thus the spanwise lift distribution should be known a priori when making the wave-drag estimate. Next, the local critical Mach number is found using Eq. (17), and the cross-sectional wave-drag coefficient C_{dw} is found using Eq. (15). Finally, the three-dimensional wave drag is calculated using Eq. (16).

By summing the contributions of all the strips, the total wave drag is found. The wave drag is calculated only for the wing. For a typical fineness ratio of 8, the body critical Mach number M_{cr} is above 0.9 [51], and thus the wave drag due to bodies can be neglected. This puts some constraints on the current model but still captures the main compressibility effect for conventional lifting-surface-based configurations. The following section provides validation for this assumption for a fuselage at $M = 0.8$.

Note that Grasmeyer [58] used this method for prediction of the Boeing 747 drag rise. The comparison shows good agreement, thus validating the method. The following sections further validate this model together with all other presented drag prediction models.

IV. Model Validation

Validation of the current model was achieved by comparing the model predictions with three different wind-tunnel tests. The first case is an experiment of a subsonic isolated wing [14], the second is a transonic swept-wing test [15], and the third is a wing/fuselage-configuration wind-tunnel test [16]. All test configurations were modeled using the current parametric geometry and then analyzed using the drag estimation methods described above.

A. Subsonic Wing Case

A wind-tunnel test of an isolated, planar, elliptic wing was conducted as part of a low induced-drag wing design work by Smith [14]. The wing is characterized by 1.829 m span, 0.502 m^2 area, and an NACA 0012 airfoil section. The test was conducted in a low-speed wind tunnel at a Mach number of $M = 0.18$ and average chord Reynolds number of $Re_{c_{\text{avg}}} = 1.12 \times 10^6$. Transition strips were located at $x/c = 0.15$ of the chord. The wing is not twisted, and thus the zero-lift drag represents only the friction-drag contribution.

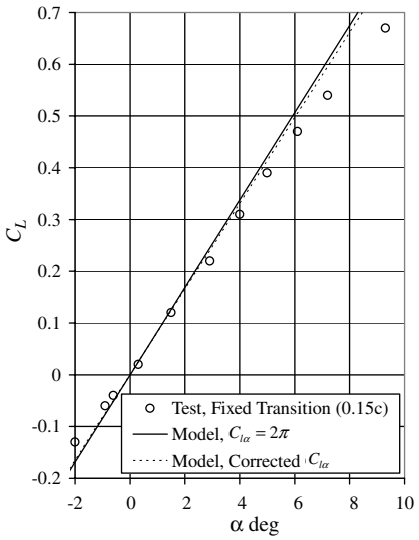

Fig. 10 Comparison between Smith's [14] lift data and current model predictions.

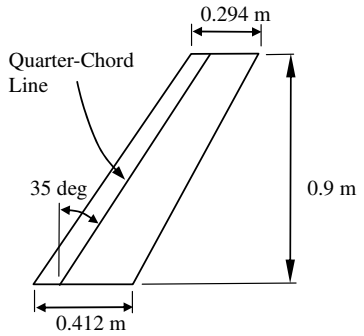

Fig. 11 Tinling and Kolk's [15] wing planform.

Although the wing is elliptic, the planform was modeled using eight spanwise trapezoid sections connected through straight lines. The induced- and friction-drag models were used to produce the comparison, which is presented in Fig. 9. This figure contains the drag polar, with a blowup of the zero-lift region. The agreement between the test results and the drag estimation is good. The friction-drag estimation can be examined by looking at the zero-lift drag region. This shows a range of eight drag counts between the various form-factor models. The test results were taken from Smith's report [14], and he reports an uncertainly of the test points of approximately 10 drag counts. Note that according to Smith's report, there is an even higher uncertainty due to the transition-strip drag.

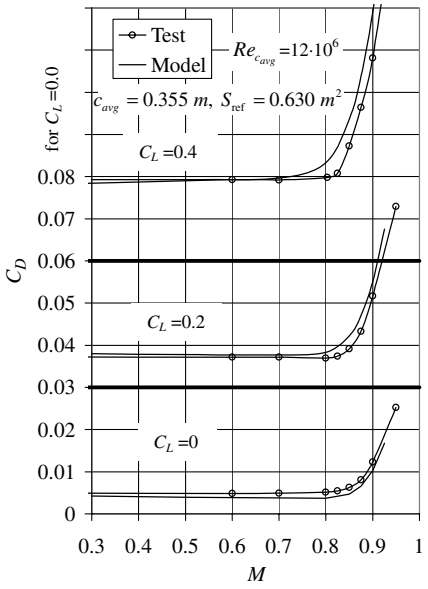

Fig. 12 Comparison of data and model predictions for the Tinling and Kolk [15] test case: Mach number influence on drag coefficient.

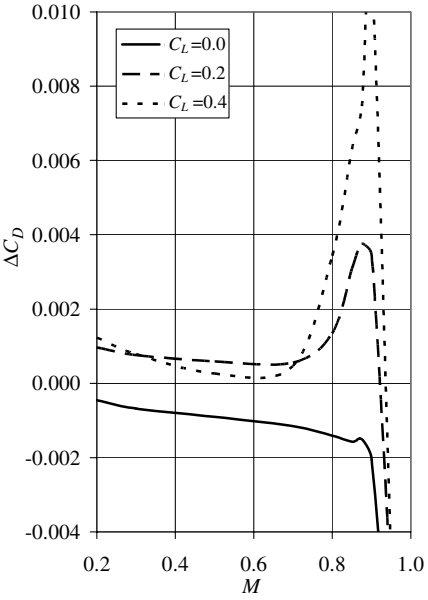

Fig. 13 Mach number influence on drag-coefficient difference between data and model predictions for the Tinling and Kolk [15] test case.

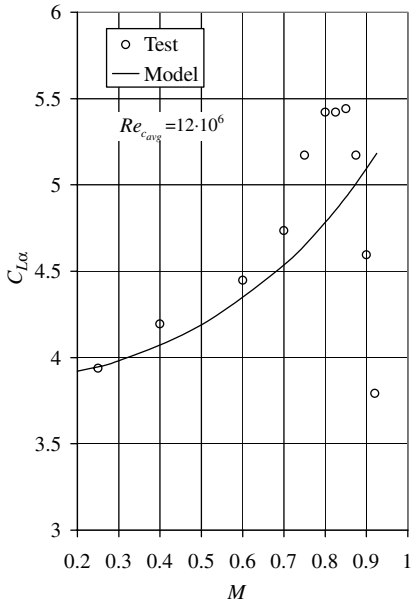

Fig. 14 Comparison of data and model predictions for the Tinling and Kolk [15] test case: lift-curve slope versus Mach number.

The drag-coefficient values for higher lift coefficients C_L agree well with the test results; thus, the induced-drag model seems to agree with the test trends. Using a constant two-dimensional curve-lift slope of $C_{l\alpha} = 2\pi$, the lift-curve (lift coefficient C_L vs angle of attack α) is presented in Fig. 10. This shows good agreement of the three-dimensional curve-lift slope and further validates the induced-drag model. Using a more accurate NACA-0012 two-dimensional curve-lift slope (from [33]), $C_{l\alpha} = 5.88$, improves the agreement even more. Note that the two-dimensional curve-lift slope does not affect the drag-polar calculation.

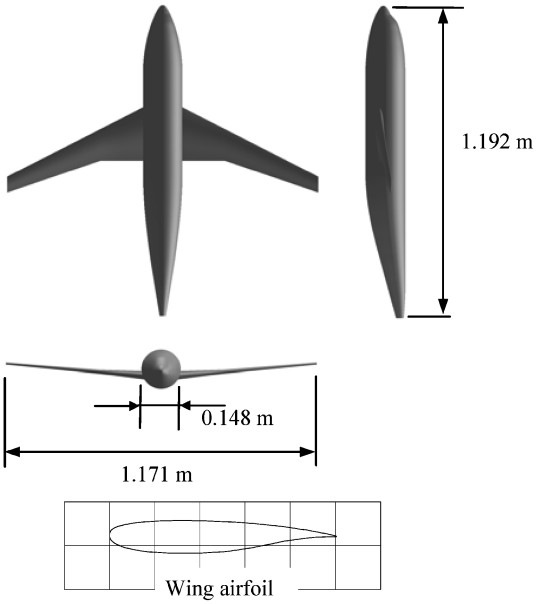

Fig. 15 DLR-F4 case geometry.

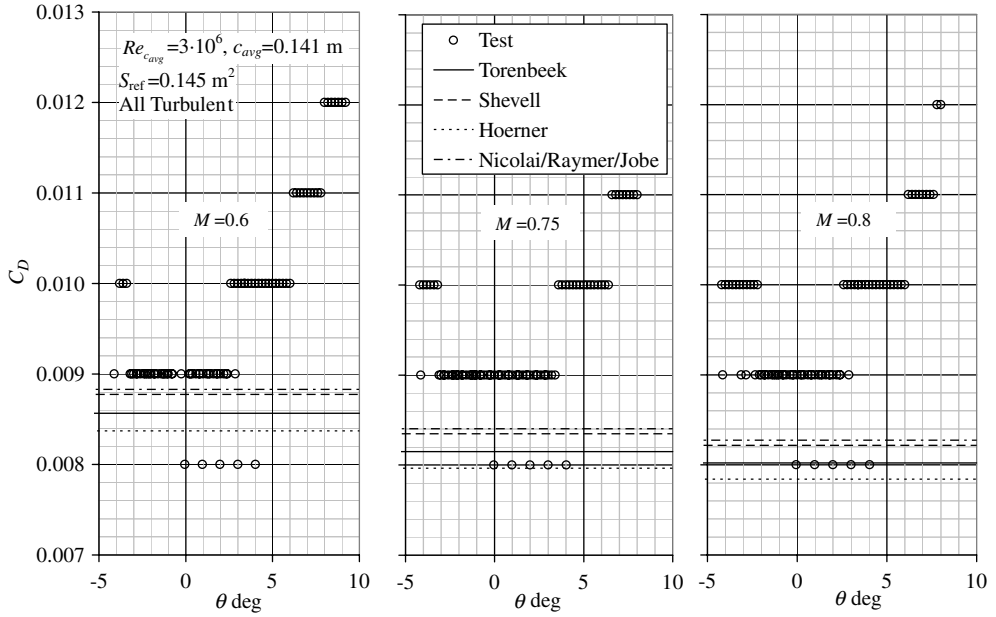

Fig. 16 Comparison of data and model predictions for DLR-F4 test case: fuselage drag coefficient at three Mach numbers.

B. Transonic Wing Case

The previous comparison was used to validate the induced- and friction-drag models. Validation of the compressibility model through the wave-drag model was done by comparing the model results with transonic swept-wing wind-tunnel test data from Tinling and Kolk [15]. Tinling and Kolk used six different wing models, all having a 35 deg quarter-chord sweep. The current comparison uses results for the wing of aspect ratio AR = 5 and symmetric 12% thickness cross section, 65_1A012, shown in Fig. 11. The test was conducted in a pressure wind tunnel at constant Reynolds number $Re_{c_{\text{avg}}} = 12 \times 10^6$ (based on the average chord $c_{\text{avg}} = 0.355$ m). The wing does not include a transition trip; thus, the transition location was found using TF = 0 and the curve defined in Fig. 5.

Figure 12 presents the wing total drag coefficient C_D as a function of Mach number M. This drag coefficient includes the induced, friction, and wave drag. Examining the zero-lift drag at low subsonic Mach numbers again validates the friction/form drag model. The current drag model uses the Raymer form factor (6) and exhibits a difference of less than 10 drag counts. In addition, the test results were digitized directly from the NACA report with a tolerance of about 10 drag counts, which is in the same order of magnitude of the model prediction error.

According to the wave-drag model, Mach number increase causes a drag increase. This trend is predicted well in Fig. 12, thus validating the drag divergence Mach M_{DD} prediction: namely, Korn equation (18). Tinling and Kolk's [15] wing uses an NACA 6 series airfoil, and thus the model used $\kappa_A = 0.87$. A higher value of κ_A would have actually improved the comparison.

Figure 12 validates the induced-drag model as well. This is done by comparing the drag coefficient C_D at three different lift coefficients C_L. Figure 13 presents the difference of the drag coefficient between the model and test results for different lift-coefficient values. For zero-lift ($C_L = 0$), good agreement is achieved up to $M = 0.9$ ($\Delta C_D = 20$ drag counts). As the lift coefficient increases, the maximum Mach number that gives good agreement decreases. For

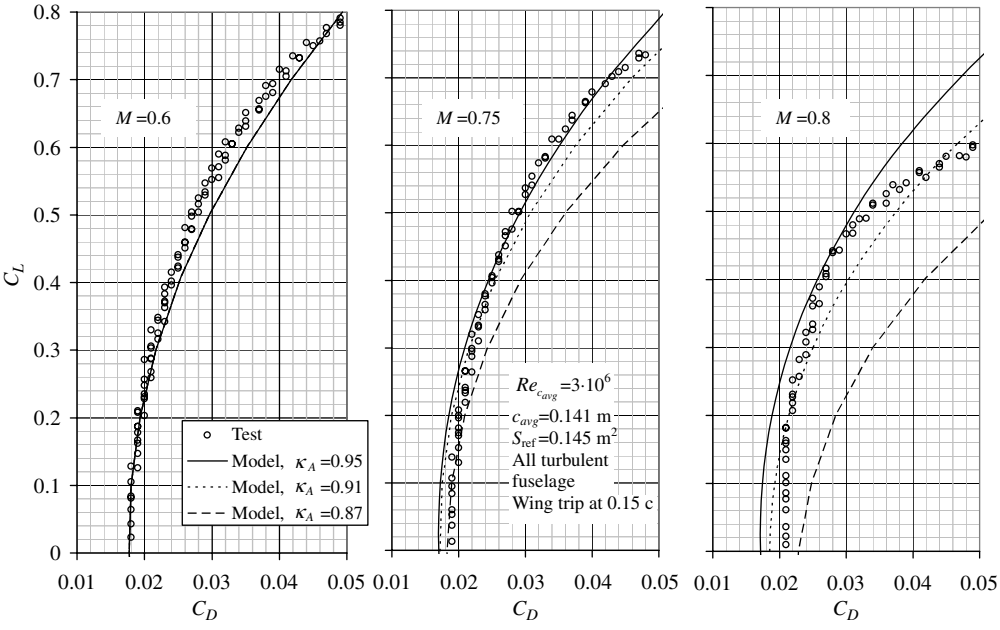

Fig. 17 Comparison of data and model predictions for DLR-F4 test case: drag polar at three Mach numbers.

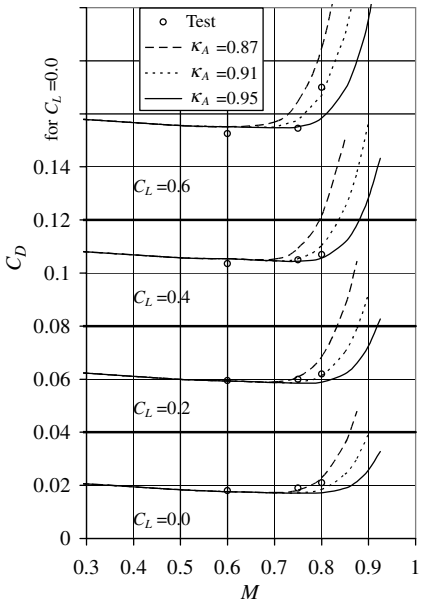

Fig. 18 Comparison of data and model predictions for DLR-F4 test case: drag coefficient vs Mach number.

$C_L = 0.2$, $\Delta C_D = 20$ at $M = 0.82$, and for $C_L = 0.4$, $\Delta C_D = 20$ at $M = 0.76$

As mentioned before, the induced-drag model uses the two-dimensional lift $C_{l\alpha}$. To correct the data for compressibility effects, a simple Prandtl–Glauert correction for a swept wing is used:

$$C_{l\alpha} = \frac{2\pi}{\sqrt{1 - M^2 \cos^2 \Lambda_{0.25}}} \tag{19}$$

This way, although the Weissinger nonlinear lifting-line is incompressible in nature, it can capture compressibility effects. This simple compressibility correction is valid for the low transonic regime, $M > 0.7$, as shown in Fig. 14.

Figure 14 shows the influence of Mach number on the three-dimensional lift slope $C_{L\alpha}$. The compressibility effect is predicted with good accuracy up to the critical Mach number; for higher Mach numbers, the simple Prandtl–Glauert correction is not applicable. Note that even though the lift-slope data and model prediction are in poor agreement at high Mach numbers, the drag estimation exhibits good results. In many situations (e.g., performance calculations), the most important measure is the drag polar rather than the lift characteristics. This implies that the current model can be used for performance predictions in the transonic regime, although its lift prediction capabilities at these conditions are somewhat poor.

C. Wing—Body Configuration Case

The first AIAA Drag Prediction Workshop (DPW) [5] followed by the second [6] and third [7] DPW used a test case from [16] of a wing/fuselage configuration denoted as DLR-F4. This configuration was tested in three different wind tunnels at three transonic Mach numbers through a range of pitch angles θ. The DLR-F4 configuration consists of a tapered swept wing and a typical transport-shaped fuselage (Fig. 15). The wing has an aspect ratio of AR = 9.5, leading-edge sweep angle of $\Lambda_{\mathrm{LE}} = 27.1$ deg, and dihedral angle of 4.8 deg. It is tapered, $\lambda = 0.3$, twisted with tip washout of 2.8 deg, and has asymmetric cross sections. The fuselage fineness ratio is $l/d = 8.0$, based on maximum diameter. The current geometry representation uses circular cross sections for the fuselage geometry; thus, the superellipse sections use zero powers, $m_U = m_L = n_U = n_L = 0$. The test was conducted at an average chord Reynolds number of $Re_{c_{\mathrm{avg}}} = 3 \times 10^6$ ($c_{\mathrm{avg}} = 0.141$ m) with the wing tripped at $x/c = 0.15$ and the fuselage tripped at the nose.

Figure 16 shows the comparison of the isolated fuselage drag coefficient for different pitch angles θ. The drag prediction is based only on the friction-drag model using different form factors. Agreement of the friction model with the test results is good, even though it does not take into consideration pitch angle or compressibility effects. Thus, the drag coefficients presented in Fig. 16 are constant. This is a reasonable approximation, demonstrating that the dependency of fuselage drag on pitch angle is small (~10 drag counts for 5 deg of pitch angle). Note that the uncertainty of the test results is 10 drag counts. The fineness ratio of the body is 8.0, and thus the range of drag prediction due to the different form factors is small (~5 drag counts).

The three-dimensional drag polar (C_L vs C_D) is presented in Fig. 17 for three different Mach numbers. The current model prediction uses Shevell's wing form factor and Torenbeek's body form factor. The agreement of the results at low Mach number implies that the wing friction-drag prediction is accurate. This is also supported by the accurate prediction of the fuselage drag (Fig. 16). The wing cross section (Fig. 15) features some supercritical characteristics, and thus $\kappa_A = 0.91$ exhibits the best agreement rather

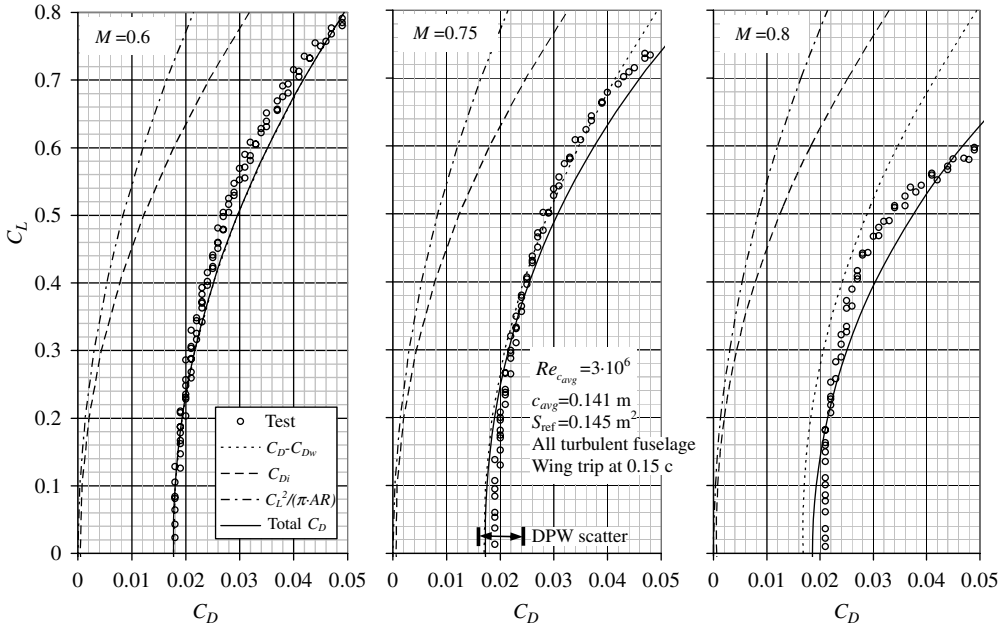

Fig. 19 Comparison of data and model predictions for DLR-F4 test case: drag polar $\kappa_A = 0.91$ at three Mach numbers.

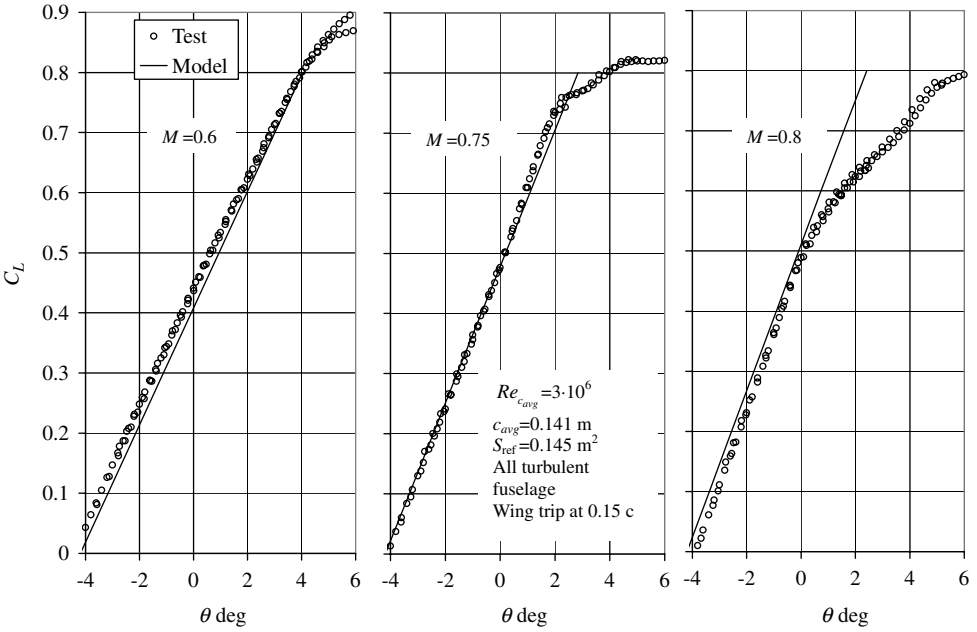

Fig. 20 Comparison of data and model predictions for DLR-F4 test case: lift coefficient vs pitch angle at three Mach numbers.

than $\kappa_A = 0.87$. Further validation of the wave-drag prediction is shown in Fig. 18, which presents the Mach number dependency of the drag coefficient for different lift coefficients C_L and Korn factors κ_A. Again, the results prove that using $\kappa_A = 0.91$ gives good agreement.

Figure 19 shows the drag breakdown of the $\kappa_A = 0.91$ polar, which is also presented in Fig. 17. The drag breakdown contains the ideal induced drag $C_L^2/(\pi \cdot \mathrm{AR})$; the actual induced drag C_{D_i}; the total drag minus the wave drag, which represents the contribution of the friction/form and interference drag, $C_D - C_{D_w}$; and the total drag C_D. Note that the contribution of the interference drag is small.

The induced-drag model is validated through the trends of the drag polars (Fig. 19) and the lift-curve slopes (Fig. 20). Note that Eq. (19) is used for prediction of the two-dimensional lift-curve slopes C_{l_α}, and a two-dimensional zero-lift angle of 2.8 deg is used. In Fig. 19 a representative scatter range of the CFD results from the DPW for $C_L = 0$ is shown [5]. This scatter range emphases the utility of the current simplified method.

V. Conclusions

A comprehensive, simple, and rapid method for estimating the drag of aircraft configurations is presented for use in transonic conceptual design, which is especially well suited for MDO. The method is used to estimate various configurations in the transonic flow regime.

The drag estimation method uses a parametric geometry that models the winglike surfaces and body entities separately. The wing surfaces are modeled using a linear interpolation between neighboring cross sections that are modeled using just the chord and thickness-to-chord ratio. Note that the parametric geometry does not include detailed cross-sectional shapes, but just the chord and thickness ratio, which simplified the problem. Although the method does not include detailed airfoil shapes, it is shown to provide a good estimation of the three-dimensional drag polar, which is lessened at high lift coefficients and high transonic Mach numbers.

Bodies are modeled using a similar method, except that the cross section's definition is done using superellipses. The main disadvantage of the suggested parametric geometry is the linear relation between the different sections; thus, modeling a continuous planform or fuselage is done by discretization using trapezoids. Nevertheless, using this parametric geometry, one can accurately model elaborate geometries simply with a small number of parameters.

The drag model uses different schemes for wings and bodies, similar to the separation done by the parametric geometry. The drag bookkeeping consists of four different components: induced, friction/form, wave, and interference drag.

The induced drag is modeled using the Weissinger nonlinear lifting-line method. The induced drag is found using simple vortex systems that represent the lifting line and its wake. Using the induced-velocity model and two-dimensional lift-coefficient data, the lift and induced-drag distribution are found. Note that this model can capture compressibility and viscosity effects through the cross section's lift data. This property was demonstrated using a simple Prandtl-Glauert correction of the two-dimensional lift slope. Using this correction, the three-dimensional lift slope is well predicted for subcritical Mach numbers ($M < M_{\mathrm{cr}}$). For higher Mach numbers, the agreement deteriorates. Nevertheless, the two-dimensional lift-curve slope has a negligible effect on the three-dimensional drag polar. The induced-drag model is not suitable for high angle of attack when severe separation occurs. Some low stall angles can be estimated using nonlinear two-dimensional lift data. The current paper does not explore this possibility.

The friction-drag model is based on semi-empirical flat-plate skin-friction models together with form-factor models. As with the parametric geometry, the friction drag is calculated differently for wings and bodies, using different form-factor models. A comparison of several common form-factor models is presented, and it is shown that the difference between these models is small, reaching, at most, 10 drag counts for average configurations. High-thickness-ratio wings or low-fineness-ratio bodies show a higher difference.

The drag contribution of bodies is limited to the friction-drag component alone. For the current method, body drag does not include compressibility effects, pitch angles, or separation. It seems that this might impose limitations on the model, but according to the presented validation for streamlined fuselages, the influences of compressibility, pitch angle, or separation are small.

Wave drag is predicted using Lock's fourth-order law and the Korn equation. Sensitivity to the Korn factor is high, and thus an accurate value for this factor is important. The model is limited to transonic speeds that are appropriate for transonic transports cruising near the drag divergence Mach number, and it is accurate in this regime.

Interference drag is modeled using mixed CFD-based and empirical models. There is a shortage of available interference models for average-thickness-ratio wings. Still, the effect of interference drag for wing/body configurations is small.

The present model can predict drag with good accuracy and capture the main aerodynamic trends affecting the configuration drag, validated through different data comparisons. Still, there are several limitations to the present model that should be considered

during its use. For example, the model does not take into account flow separation, and thus it is not suitable for high-angle-of-attack subsonic analysis. This means that the current method should be used mainly in the conceptual-design phase or at later design stages as part of a multifidelity drag estimation method, incorporating high-fidelity methods (such as CFD) with the current efficient method.

Note that various aerodynamic influences are not taken into account in the current scope, such as propulsion effects or high-lift devices. These influences can be included in future versions of this model.

Acknowledgments

The authors would like to acknowledge the support of NASA Langley Research Center. The authors thank Dimitri Mavris, Taewoo Nam, and Hongjun Ran from Georgia Institute of Technology for their contribution to the Vehicle Sketch Pad (VSP) implementation.

References

[1] Hoerner, S. F., *Fluid Dynamic Drag*, Hoerner Fluid Dynamics, Bakersfield, CA, 1965.

[2] Prandtl, L., "Tragfliigeltheorie," *Nachrichten von der Gesellschaft der Wissenschaften zu Göttingen*, Pt. 1, 451–477, 1918.

[3] Prandtl, L., "Tragfliigeltheorie," *Nachrichten von der Gesellschaft der Wissenschaften zu Göttingen*, Pt. 2, 107–137, 1918.

[4] van Dam, C. P., "Recent Experience with Different Methods of Drag Prediction," *Progress in Aerospace Sciences*, Vol. 35, No. 8, Nov. 1999, pp. 751–798.
doi:10.1016/S0376-0421(99)00009-3

[5] Levy, D. W., Zickuhr, T., Vassberg, J., Agrawal, S., Wahls, R. A., Pirzadeh, S., and Hemsch, M. J., "Summary of Data from the First AIAA CFD Drag Prediction Workshop," 40th AIAA Aerospace Sciences Meeting and Exhibit, AIAA Paper 2002-0841, Reno, NV, Jan. 2002.

[6] Laflin, K., Klausmeyer, S. M., Zickuhr, T., Vassberg, J. C., Wahls, R. A., Morrison, J. H., et al., "Data Summary from Second AIAA Computational Fluid Dynamics Drag Prediction Workshop," *Journal of Aircraft*, Vol. 42, No. 5, 2005, pp. 1165–1178.
doi:10.2514/1.10771

[7] Vassberg, J. C., Tinoco, E. N., Mani, M., Brodersen, O. P., Eisfeld, B., Wahls, R. A., Morrison, J. H., Zickuhr, T., Laflin, K. R., and Mavriplis, D. J., "Summary of the Third AIAA CFD Drag Prediction Workshop," 45th AIAA Aerospace Sciences Meeting and Exhibit, AIAA Paper 2007-0260, Reno, NV, Jan. 2007.

[8] Giunta, A. A., Golovidov, O., Knill, D. L., Grossman, B., Mason, W. H., Watson, L. T., and Haftka, R. T., "Multidisciplinary Design Optimization of Advanced Aircraft Configurations," *Lecture Notes in Physics*, edited by P. Kutler, J. Flores, and J.-J. Chattot, Vol. 490, Springer–Verlag, New York, 1997, pp. 14–34.

[9] Mason, W. H., Knill, D. L., Giunta, A. A., Grossman, B., Haftka, R. T., and Watson, L. T., "Getting the Full Benefits of CFD in Conceptual Design," AIAA 16th Applied Aerodynamics Conference, AIAA Paper 98-2513, Albuquerque, NM, June 1998.

[10] Paterson, J. H., MacWilkinson, D. G., and Blackerby, W. T., "A Survey of Drag Prediction Techniques Applicable to Subsonic and Transonic Aircraft Design," *Aerodynamic Drag*, CP-124, AGARD, Neuilly-sur-Seine, France, April 1973.

[11] Filippone, A., "Comprehensive Analysis of Transport Aircraft Flight Performance," *Progress in Aerospace Sciences*, Vol. 44, No. 3, April 2008, pp. 192–236.
doi:10.1016/j.paerosci.2007.10.005

[12] Jensen, S. C., Rettie, I. H., and Barber, E. A., "Role of Figure of Merit in Design Optimization and Technology Assessment," *Journal of Aircraft*, Vol. 18, No. 2, Feb. 1981, pp. 76–81.
doi:10.2514/3.57468

[13] Malone, B., and Mason, W. H., "Aircraft Concept Optimization Using Parametric Multiobjective Figures of Merit," *Journal of Aircraft*, Vol. 33, No. 2, March–April, 1996, pp. 444–445.
doi:10.2514/3.46960

[14] Smith, S. C., "A Computational And Experimental Study of Nonlinear Aspects of Induced Drag," NASA TP-3598, 1996.

[15] Tinling, T. E., and Kolk, R. W., "The Effects of Mach Number and Reynolds Number on the Aerodynamic Characteristics of Several 12-Percent-Thick Wings Having 35° of Sweepback and Various Amounts of Camber," NACA RM-A50K27, Feb. 23, 1951.

[16] Redeker, G., "DLR-F4 Wing Body Configuration," *A Selection of Experimental Test Cases for the Validation of CFD Codes*, Vol II, AGARD Rept. 303, Neuilly-sur-Seine, France, Aug. 1994.

[17] Rajnarayan, D., Haas, A., and Kroo, I., "A Multi-Fidelity Gradient-Free Optimization Method and Application to Aerodynamic Design," 12th AIAA/ISSMO Multidisciplinary Analysis and Optimization Conference, AIAA Paper 2008-6020, Victoria, B.C., Canada, Sept. 2008.

[18] Hicks, R., and Vanderplaats, G. N., "Design of Low-Speed Airfoils by Numerical Optimization," Society of Automotive Engineers, Paper 75024, April 1975.

[19] Davis, W. H., Jr, Aidala, P. V., and Mason, W. H., "A Study to Develop Improved Methods for the Design of Transonic Fighter Wings by the Use of Numerical Optimization," NASA CR 3995, Aug. 1986.

[20] Reneaux, J., and Thibert, J-J., "The Use of Numerical Optimization for Airfoil Design," AIAA 3rd Applied Aerodynamics Conference, AIAA Paper 85-5026, Colorado Springs, CO, Oct. 1985.

[21] Vachris, A. F., Jr, and Yaeger, L. S., "A Rapid Response Method for Mathematically Modeling Configuration Geometry," *Application of Computer Graphics in Engineering Proceeding*, NASA Langley Research Center, Hampton, VA, Jan. 1975, pp. 49–73.

[22] Kulfan, B. M., "Universal Parametric Geometry Representation Method," *Journal of Aircraft*, Vol. 45, No. 1, Jan.–Feb. 2008, pp. 142–158.
doi:10.2514/1.29958

[23] Rodriguez, D. L., and Sturdza, P., "A Rapid Geometry Engine for Preliminary Aircraft Design," 44th AIAA Aerospace Sciences Meeting and Exhibit, AIAA Paper 2006-929, Reno, NV, Jan. 2006.

[24] Barger, R. L., "An Analytical Procedure for Computing Smooth Transitions Between Two Specified Cross Sections With Applications to Blended Wing-Body Configurations," NASA TP 2012, May 1982.

[25] Gloudemans, J. R., Davis, P. C., and Gelhausen, P. A., "A Rapid Geometry Modeler for Conceptual Aircraft,", 34th AIAA Aerospace Sciences Meeting and Exhibit, AIAA Paper 1996-0052, Reno, NV, Jan. 1996.

[26] Dufresne, S., Johnson, C., and Mavris, D. N., "Variable Fidelity Conceptual Design Environment for Revolutionary Unmanned Aerial Vehicles," *Journal of Aircraft*, Vol. 45, No. 4, July–Aug. 2008, pp. 1405–1418.

[27] Feagin, R. C., and Morrison, W. D., Jr, "Delta Method: An Empirical Drag Buildup Technique," NASA CR 151971, Dec. 1978.

[28] Blackwell, J., "Numerical Method To Calculate the Induced Drag or Optimal Span Loading for Arbitrary Non-Planar Aircraft," NASA SP-405, May 1976.

[29] Falkner, V., "The Solution of Lifting-Plane Problems by Vortex-Lattice Theory," Aeronautical Research Council Reports and Memoranda No. 2591, London, 1943.

[30] Weissinger, J., "The Lift Distribution of Swept-Back Wings," NACA TM 1120, March 1947.

[31] Owens, B. D., "Weissinger's Model of the Nonlinear Lifting-Line Method for Aircraft Design," 36th Aerospace Sciences Meeting and Exhibit AIAA Paper 1998-0597, Reno, NV, Jan. 1998.

[32] McCormick, B. W., "An Iterative Non-Linear Lifting-Line Model for Wings with Unsymmetrical Stall," *General Aviation Aircraft Meeting and Exposition*, Society of Automotive Engineers, Paper 891020, Wichita, KS, April 1989.

[33] McCroskey, W. J., "A Critical Assessment of Wind Tunnel Results for the NACA 0012 Airfoil," NASA TM-100019, Oct. 1987.

[34] Gur, O., Mason, W. H., and Schetz, J. A., "Full Configuration Drag Estimation," 27th AIAA Applied Aerodynamics Conference AIAA Paper 2009-4109, San Antonio, TX, June 2009.

[35] Schultz-Grunow, F., "Neues Reibungswiderstandsgesetz für Glatte Platen," *Luftfahrtforschung*, Vol. 17, No. 8, Aug. 1940, pp. 239–246; "New Frictional Resistance Law for Smooth Plates," NACA TM-986, 1941 (English translation).

[36] Spalding, D. B., and Chi, S. W., "The Drag of a Compressible Turbulent Boundary Layer on a Smooth Flat Plate with and Without Heat Transfer," *Journal of Fluid Mechanics*, Vol. 18, Part 1, 1964, pp. 117–143.
doi:10.1017/S0022112064000088

[37] White, F. M., *Viscous Fluid Flow*, McGraw–Hill, New York, 1974.

[38] Hopkins, E. J., and Inouye, M., "An Evaluation of Theories for Predicting Turbulent Skin Friction and Heat Transfer on Flat Plates at Supersonic and Hypersonic Mach Numbers," *AIAA Journal*, Vol. 9, No. 6, June 1971, pp. 993–1003.
doi:10.2514/3.6323

[39] Hopkins, E. J., "Charts for Predicting Turbulent Skin Friction from the Van Driest Method (II)," NASA TN D-6945, Oct. 1972.

[40] Liu, C., "Drag of a Flat Plate with Transition in the Absence of Pressure Gradient," *Journal of Aircraft*, Vol. 9, No. 7, July 1972, pp. 509–510.
doi:10.2514/3.59026

[41] Collar, A. R., "A Closed Formula for the Drag of a Flat Plate with Transition in the Absence of a Pressure Gradient," *Journal of the Royal Aeronautical Society*, Vol. 64, Jan. 1960, pp. 38–39.
[42] Cebeci, T., and Bradshaw, P., *Momentum Transfer in Boundary Layers*, McGraw–Hill, New York, 1977.
[43] Mason, W. H., "Boundary Layer Analysis Methods," *Aerodynamic Calculation Methods for Programmable Calculators & Personal Computers*, PAK 4 AEROCAL, Huntington, NY, 1981.
[44] Braslow, A. L., Bartlett, D. W., Wagner, R. D., and Collier, F. S., Jr, "Applied Aspects of Laminar-Flow Technology," *Viscous Drag Reduction in Turbulent Boundary Layers*, Progress in Aeronautics and Astronautics, edited by D. M. Bushnell, and J. N. Hefner, AIAA, New York, 1990.
[45] Boltz, F. W., Kenyon, G. C., and Allen, C. Q., "Effects of Sweep Angle on the Boundary-Layer Stability Characteristics of an Untapered Wing at Low Speeds," NASA TN D-338, Oct. 1960.
[46] Wagner, R. D., Bartlett, D. W., and Collier, F. S., Jr, "Laminar Flow—The Past, Present, and Prospects," 2nd AIAA Shear Flow Conference AIAA Paper 1989-0989, Tempe, AZ, March 1989.
[47] Torenbeek, E., *Synthesis of Subsonic Airplane Design*, Delft Univ. Press, Delft, The Netherlands, and Martinus Nijhoff, Hague, The Netherlands, 1982.
[48] Jobe, C. E., "Prediction and Verification of Aerodynamic Drag, Part I: Prediction," *Thrust and Drag: Its Prediction and Verification*, Progress in Astronautics and Aeronautics, edited by C. E. Eugene, Vol. 98, AIAA, New York, 1985, Chap. 4.
[49] Shevell, R. S., *Fundamentals of Flight*, Prentice–Hall, Upper Saddle River, NJ, 1989.
[50] Nicolai, M. L., *Fundamentals of Aircraft Design*, E. P. Domicone, Fairborn, OH, 1975.
[51] Raymer, D. P., *Aircraft Design: A Conceptual Approach*, AIAA Education Series, AIAA, Reston VA, 2006.
[52] Tétrault, P.-A., "Numerical Prediction of the Interference Drag of a Streamlined Strut Intersecting a Surface in Transonic Flow," Ph.D. Thesis, Virginia Polytechnic Inst. and State Univ., Jan. 2000.
[53] Tétrault, P.-A., Schetz, J. A., and Grossman, B., "Numerical Prediction of the Interference Drag of a Strut-Surface Intersection in Transonic Flow," *AIAA Journal*, Vol. 39, No. 5, May 2001, pp. 857–864. doi:10.2514/2.1389
[54] Shevell, R. S., "Aerodynamic Bugs: Can CFD Spray Them Away?," 3rd Applied Aerodynamics Conference, AIAA Paper 1985-4067, Colorado Springs, CO, Oct. 1985.
[55] Inger, G. R., "Application of Oswatitsch's Theorem to Supercritical Airfoil Drag Calculation," *Journal of Aircraft*, Vol. 30, No. 3, May–June 1993, pp. 415–416. doi:10.2514/3.46354
[56] Hilton, H. W., *High Speed Aerodynamics*, Longmans, Green, London, 1951.
[57] Mason, W. H., "Analytic Models for Technology Integration in Aircraft Design," AIAA/AHS/ASEE Aircraft Design, Systems and Operations Conference, AIAA Paper 90-3263, Dayton, OH, Sept. 1990.
[58] Grasmeyer, J., "Multidisciplinary Design Optimization of a Transonic Strut-Braced Wing Aircraft," 37th AIAA Aerospace Sciences Meeting and Exhibit, AIAA Paper 99-16010, Reno, NV, Jan. 1999.